ARTICLE

Surface Formation of Single Silicon Wafer Polished with Nano-sized Al_2O_3 Powders†

Yu-li Sun, Dun-wen Zuo*, Yong-wei Zhu, Min Wang

College of Mechanical and Electrical Engineering, Nanjing University of Aeronautics and Astronautics, Nanjing 210016, China

(Dated: Received on July 23, 2007; Accepted on October 10, 2007)

Ice polishing single silicon wafers with nano-sized Al_2O_3 abrasives can be known as ice fixed abrasives chemical mechanical polishing (IFA-CMP). TAn abrasive slurry was made of nano-sized Al_2O_3 particles dispersed in de-ionized water with a surfactant and the slurry was frozen to form an ice polishing pad. Then polishing tests of blanket silicon wafers with the above ice polishing pad were carried out. The morphologies and surface roughness of the polished silicon wafers were observed and examined on an atomic force microscope. The subsurface damage was assessed by means of cross-section transmission electron microscopy. The surface chemical constituents of the polished silicon wafers were characterized using X-ray photoelectron spectroscopy in order to gain insight into the chemical mechanisms in the process. Scratch resistance of the single silicon wafer was measured by nanoscratching using a nanoindenter to explore the mechanical removal mechanism. The results show that a super smooth surface with an average roughness of 0.367 nm is obtained within 1000 nm×1000 nm and there is a perfect silicon diamond structure without any microcracks in the subsurface. The removal of material is dominated by the coactions of ductile regime machining and chemical corrosion. In the end, a model of material removal of IFA-CMP is built.

Key words: Single silicon wafer, Nano-sized Al_2O_3, Ice fixed abrasives CMP, Nanoscratch, Ductile regime machining

I. INTRODUCTION

With the development of ULSI, device dimensions are becoming smaller and smaller, and the diameters of silicon wafer used as substrate materials are becoming larger and larger (up to ϕ300 mm). The requirements for total and local thickness variations of silicon wafer are becoming stricter and stricter [1,2] and the silicon wafers not only need to have very good flatness and low surface roughness but also have no surface damage or scratches. Single crystal Si has a covalently bonded diamond structure which makes it difficult to slip over one to another, which results in fracture when a Si wafer is subjected to a severe stress under various processes. Cracks are observed on the processed Si surface [3], so it is difficult to machine it. Chemical mechanical polishing (CMP) was first put forward in 1967 by IBM [4] and gradually replaced the traditional methods, such as single chemical polishing or single mechanical polishing. Because CMP not only makes a better surface, but also provides higher polishing rate and flatness, it is commonly recognized to be the best and only method of achieving global planarization of topography with a low post-planarization slope [5-8] and has attracted more and more attention from researchers [9-17]. The CMP process is widely used, yet there is only a limited understanding of the fundamental mechanisms involved. Fundamental research has been done to both experimentally understand polishing characteristics and analytically model the process involved [18-20]. New technologies offer new opportunities for process integration apart from CMP. Some researches find that many defects of the machined surface, such as residual stress, micro-cracks and surface damages, can be decreased in ice conditions [21-23]. In recent years, some polishing tests of blanket silicon wafers, glass ceramics and metal-base nickel coating with ice polishing pads containing colloidal SiO_2 have been carried out and a smooth surface with an average roughness of 1.29 nm for single silicon wafer has been obtained [24,25]. However, few polishing tests with respect to the blanket silicon wafers with ice polishing pad containing nano-sized Al_2O_3 have been conducted and the ice polishing mechanisms have not been studied deeply in the field of semiconductor.

This work reports some polishing tests with respect to the single silicon wafers in the presence of the ice polishing pad containing nano-sized Al_2O_3 and investigates the ice polishing effect and mechanism.

II. EXPERIMENTS

As Fig.1 shows, the ice fixed abrasives CMP (IFA-CMP) was performed on a wafer polisher with an ice pad. During the polishing experiment, the wafer was mounted on an object carrier with a diameter of 76.2 mm. The applied pressure was controlled by an air cylinder. The down force pressure was kept at 0.05 MPa

†Part of the special issue from "The 6th China International Conference on Nanoscience and Technology, Chengdu (2007)".

*Author to whom correspondence should be addressed. E-mail: imit505@nuaa.edu.cn , Fax: +86-25-84890779

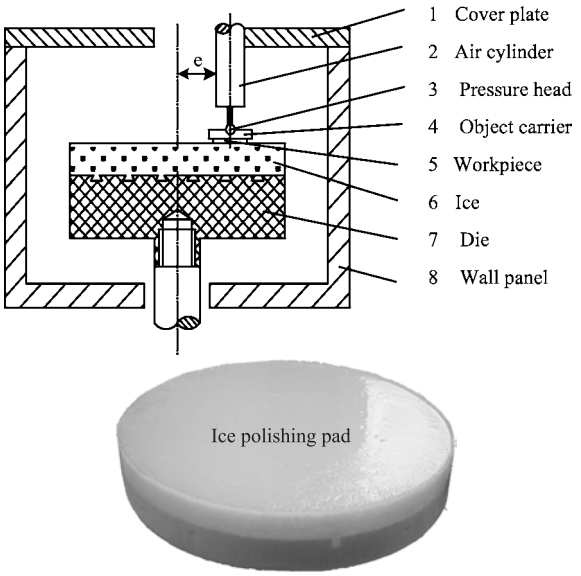

FIG. 1 Schematic diagram of ice polishing apparatus.

and the polisher rotated at 400 r/min. The eccentricity was kept at 10 mm and the polishing time was 60 min.

Single-crystal Si(100) wafers with a diameter 76.2 mm. were chosen in this study. The abrasive slurry was made of nano-sized Al_2O_3 particles dispersed in de-ionized water with a surfactant. The particles used had a primary diameter of about 20 nm with a purity level of more than 99.9%. The surfactant sodium oleate (0.05%) was added to get a stable suspension. The concentration of Al_2O_3 was 1%. Ammonia water was used to regulate the pH value of the slurry and the pH value (measured by PHS-3C at 18 °C) of the slurry was fixed at 11 to get the most stable suspension. The suspension was characterized by TEM. As shown in Fig.2, the mean diameter of the Al_2O_3 particles in the slurry is about 60 nm and their shape is approximately spherical. Then the polishing slurry was frozen in a die to form an ice polishing pad, as shown in Fig.1. For comparison, silicon wafers were prepared with conventional procedures as rough lapping with 305♯ and 303♯ silicon carbide, fine lapping with 302♯ silicon carbide and pre-polishing with 2.6 and 0.8 μm CeO_2 abrasives. The morphologies and surface roughness of the polished silicon wafers were observed and examined on an AFM (CSPM-4000). The AFM morphology of the pre-polished silicon wafer surface is shown in Fig.3(a). It can be seen that the waveness is bigger and there are some tubercles. The chemical reaction between the thin liquid film (formed between the ice polishing pad and silicon wafer during the superficial coat of the ice polishing pad thawing) and the silicon wafer was evaluated by using X-ray photoelectron spectroscopy (XPS) for phase identification. The mechanical removal mechanism of the single silicon wafer was characterized by nanoscratch technique using

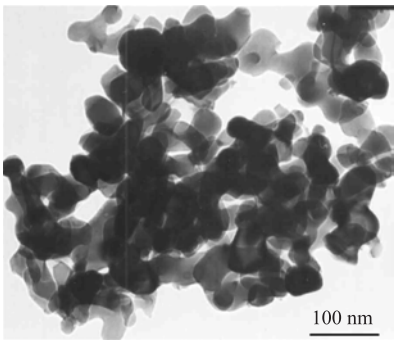

FIG. 2 TEM image of Al_2O_3 particles.

a Nano Indenter XP (MTS Systems Corp.) equipped with the lateral force measurement (LFM) option. In nanoscratch studies, a three-sided pyramidal diamond (Berkovich) indenter, having a tip radius of about 100 nm and an included angle of 65.2°, was drawn over the sample surface, and the load was ramped up, until substantial damage occurred. The coefficient of friction was monitored during scratching. In order to obtain scratch depths during scratching, the surface profile of the silicon wafer was first obtained by scanning the sample at a low load of about 100 μN, which is insufficient to damage the sample surface. The 500 μm long scratches were made by scanning the sample while ramping the loads on the three-sided pyramidal tip over different loads from 100 μN to 200 mN. The actual depth during scratching was obtained by subtracting the initial profile from the scratch depth measured during scratching. In order to measure the scratch depth after the scratch, the scratched surface was profiled at a low load of 100 μN and was subtracted from the actual surface profile before scratching [26-29].

III. RESULTS AND ANALYSIS

A. AFM and TEM evaluation

The surface roughness of silicon wafer within different dimensions is shown in Table I. The surface roughness of the silicon wafer polished with 60 nm Al_2O_3 particles is obviously smaller than that of pre-polished and a super smooth surface with an average roughness of 0.367 nm is obtained within 1000 nm×1000 nm. The AFM morphology of the silicon wafer surface polished with nano-sized Al_2O_3 particles within 10000 nm×10000 nm is shown in Fig.3(b). The waveness of polished surface is smaller and there are few tubercles. As shown in Fig.3(c), TEM studies of the subsurface structure demonstrate a perfect silicon diamond structure without any microcracks. These perfect surface and subsurface benefited from the special ice polishing mechanism.

DOI:10.1088/1674-0068/20/06/643-648

TABLE I Properties of NiO-CeO_2 and Bi_2O_3-CeO_2 compounds

Surface states	1000 nm×1000 nm		5000 nm×5000 nm		10000 nm×10000 nm	
	R_a/nm	RMS/nm	R_a/nm	RMS/nm	R_a/nm	RMS/nm
Pre-polished	0.502	0.773	0.934	1.790	1.030	2.420
Polished with Al_2O_3 slurry	0.367	0.517	0.516	0.935	0.568	0.997

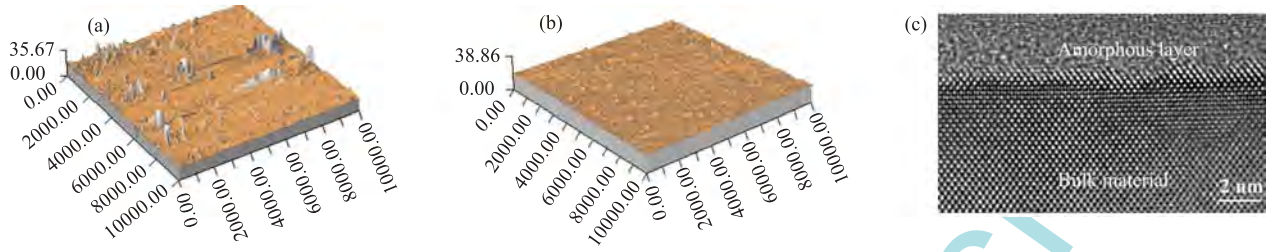

FIG. 3 Patterns of the silicon wafer. (a) AFM morphology of the pre-polished silicon wafer surface (within 10000 nm×10000 nm), (b) AFM morphology of the polished silicon wafer surface (within 10000 nm×10000 nm), (c) TEM sectional image of the polished silicon wafer.

B. Polishing mechanism of IFA-CMP

When making the ice polishing pad, the bonding agent was de-ionized water and the abrasives were frozen into an ice pad, so the ice pad can be known as an ice fixed abrasives polishing pad (IFA-PP). During the ice polishing, though the temperature of the polishing pad was very low, the local temperature in the working area was about 3-5 °C. According to the theory of tribochemistry [30, 31], high temperature and high pressure can form at the local contact point between the abrasives and the silicon wafer during the polishing, so the temperature at the contact point can be greater than 0 °C and there will be a thin liquid film between the ice polishing pad and silicon wafer after the superficial coat of the polishing pad thaws. As the polishing process goes on unceasingly, the abrasives in the superficial coat of the polishing pad can pull off and the new ones can emerge continuously. Therefore, this IFA-PP has the ability of self-dressing. Another result of the high-temperature and high-pressure formed at the local contact point between the abrasives and the silicon wafer during the polishing is that it can cause a series of tribochemical reactions. Under alkaline condition, there will be a soft corrosion layer formed on the surface of the silicon wafer and then the soft corrosion layer will be removed by mechanical action of the abrasives, simultaneously, new surface will emerge. In addition, this chemical-mechanical reaction process cycles.

C. Chemical reaction

The pH value (measured at 18 °C) of the polishing wastes was 10.15 and this means that chemical reaction occurred during IFA-CMP. The X-ray photoelectron spectroscopy technique was employed in order to make clear the mechanism of the chemical reaction under IFA-CMP process. Figure 4 shows the Si2p XPS peaks from a silicon wafer surface after being polished with ice polishing pad. The binding energies associated with the Si2p XPS peaks are 98.91 and 102.47 eV. The value 98.91 eV is in good agreement with Si, p-type and there is no suitable formula that is in agreement with 102.47 eV in the XPS database. This indicates that there is some new substance formed on the surface of the wafer and the new substance may be the soft corrosion layer. Removal of silicon during CMP is explained by an attack of OH^- to silicon atoms catalyzing the corrosive reaction of H_2O resulting in cleavage of silicon bonds [5,32]. The chemical equation is the following:

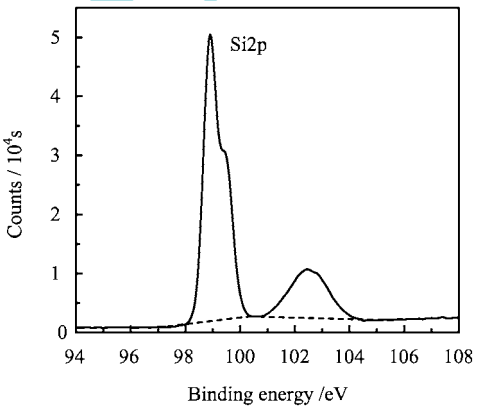

FIG. 4 Si2p XPS peaks from a silicon wafer surface after being polished with ice polishing pad.

$$Si + 2OH^- + H_2O \rightarrow SiO_3^{2-} + 2H_2 \uparrow \quad (1)$$

DOI:10.1088/1674-0068/20/06/643-648

If SiO_3^{2-} in the slurry can not be removed immediately, SiO_3^{2-} can hydrolyze according to the following equation:

$$SiO_3^{2-} + 2H_2O \rightarrow H_2SiO_3 \downarrow + 2OH^- \quad (2)$$

The reaction between alkalis and silicate particle is as follows:

$$NH_4OH \rightarrow NH_4^+ + OH^- \quad (3)$$

$$SiO_3^{2-} + 2NH_4^+ \rightarrow H_2SiO_3 \downarrow + 2NH_3 \quad (4)$$

The resultant H_2SiO_3 can partly polymerize into hydrated silica and simultaneously another part of H_2SiO_3 can ionize to form SiO_3^{2-}. In the end, the silicate colloid $\{(SiO_2)_m \cdot nSiO_3^{2-} \cdot 2(n-x)H^+\}^{2x-} \cdot 2xH^+$ formed. The silicate colloid covering the silicon wafer surface was the main component of the soft corrosion layer. The formation of silicate colloid $\{(SiO_2)_m \cdot nSiO_3^{2-} \cdot 2(n-x)H^+\}^{2x-} \cdot 2xH^+$ in IFA-CMP process seems to be the key mechanism.

D. Mechanical action of the abrasives

Figure 5 shows the model of IFA-CMP. If the thickness of the soft corrosion layer is σ, the depth a_0 that the nano particles are embedded in the bulk of silicon wafer can be expressed as follows:

$$a_0 = a - \sigma \quad (5)$$

where a is the depth of the nano particles in the surface of the silicon wafer.

From Eq.(5), we can see that the soft corrosion layer decreases the embedding depth of the nano particles in the bulk of silicon wafer, and that there is some polishing slurry between the polishing pad and silicon wafer after the superficial coat of the polishing pad thaws. So, during polishing, a stable thin liquid film can form because of the dynamic pressure produced by the stable rotation of the object carrier and the polishing pad. As shown in Fig.5, assuming that the thickness of the liquid film is a_1, this film also has the effect of decreasing the depth that the nano particles are embedded in the bulk of the silicon wafer.

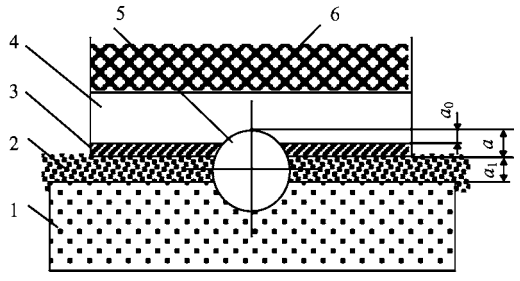

FIG. 5 Model of material removal of IFA-CMP. 1: Ice fixed abrasives polishing pad, 2: Liquid film, 3: Soft corrosion layer, 4: Bulk material, 5: Nano-sized Al_2O_3 abrasive, 6: Object carrier.

E. Nanoscratch

The scratch depth and coefficient of friction profiles as a function of increasing normal load and scratch distance and SEM images of three regions over scratches are shown in Fig.6. As shown in Fig.6, the nanoscratch includes three stages. At the first stage, when the normal load is between 0 and 76.68 mN, the scratch depth profile obtained after the scratch on the silicon wafer with respect to initial profile does not change. This is attributed to an elastic recovery after removal of the normal load. The silicon wafer exhibits a continuous increase in the coefficient of friction with increasing normal load from the beginning of the scratch. At the second stage, when the normal load is between 76.68 and 138.64 mN, the tip plows a trough via plastic deformation of the silicon wafer, leaving a ductile groove, as shown in SEM image in stage II of Fig.6. From Fig.6, reduction in scratch depth is observed after scratching as compared to during scratching. This reduction in scratch depth is attributed to an elastic recovery after removal of the normal load. The silicon wafer also exhibits a continuous increase in the coefficient of friction with increasing normal load. The continuous increase in the coefficient of friction during scratching is attributed to the increasing plowing of the sample by the tip with increasing normal load. When the normal load increases to 138.64 mN (indicated by A on the scratch depth and the friction profiles), the scratch depth profile obtained after the scratch on the silicon wafer and the coefficient of friction begin to fluctuate obviously. The SEM image of stage III shows that there are many cracks on the side of the scratch right from the load of 138.64 mN and up, which is probably responsible for the big fluctuation in the scratch depth and the friction profiles. At the end of the scratch, some of the surface material was torn away and cracks were found on the side of the scratch in the silicon wafer. The scratch depth after scratching indicates the final depth which reflects the extent of permanent damage and plowing of the tip into the sample surface, and is probably more relevant for visualizing the damage that can occur in real machining. For the Si (100), there is a large scatter in the scratch depth data after the load of 138.64 mN, which is associated with the generation of cracks, material removal and debris. Therefore, the critical load and scratch depth estimated from the scratch depth profile after the scratching and the friction profile are 138.64 mN and 54.63 nm respectively.

The transition from a brittle mode to a ductile one during the machining of brittle materials is described in terms of energy balance between the strain energy and the surface energy [33]. It was found that there was a critical grain depth of cut for the brittle-to-ductile transition. For grain depths of cut below the threshold value, the material removal process was largely ductile. For the grain depths of cut above the threshold value, the material removal process was mostly brittle.

DOI:10.1088/1674-0068/20/06/643-648

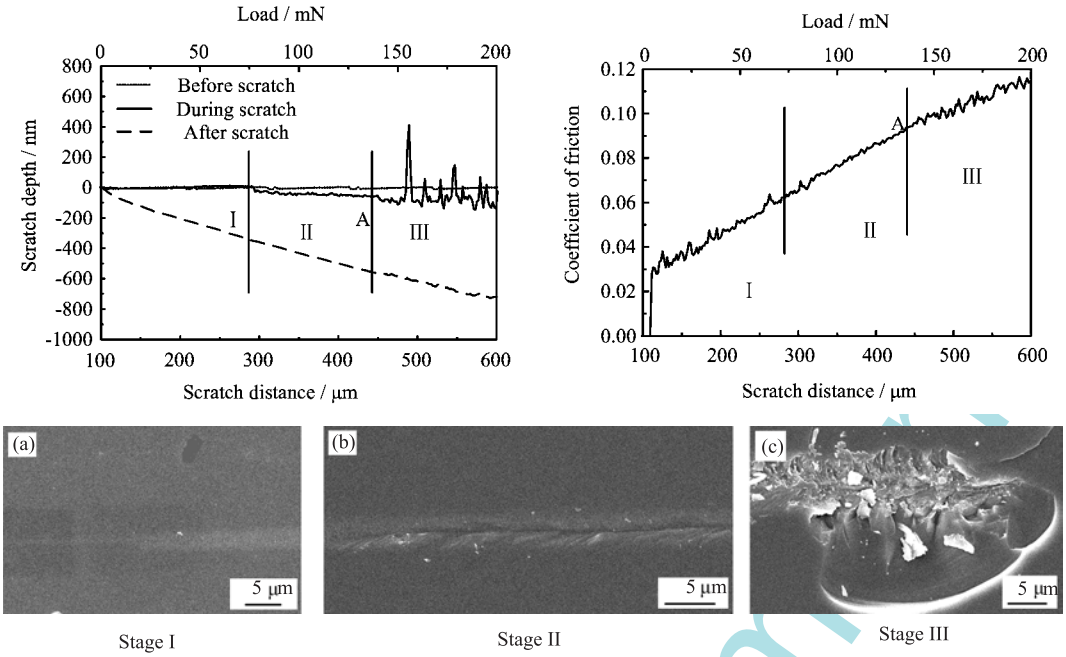

FIG. 6 Coefficient of friction and scratch depth as a function of normal load and scratch distance and SEM images of three regions over scratches.

From the nanoscratching test, it is shown that the material removal mechanisms consist of elastic deformation, plastic grooving and crushing. The material removal mechanisms are directly related to the normal force on the tip. The critical load and scratch depth estimated from the scratch depth profile after the scratching and the friction profile are 138.64 mN and 54.63 nm respectively. If the load and scratch depth are under the critical value, the silicon wafer will undergo plastic flow rather than fracture.

From the above analysis, it is shown that the Al_2O_3 abrasives in the slurry are about 60 nm in size and the soft corrosion layer forming in the polishing process can obviously decrease the embedding depth of the nano particles in the bulk of silicon wafer, so the grain depth of cut decreases. Also, through AFM evaluation we know the waveness of polished surface is smaller and there are few tubercles. Therefore, we can conclude that the grain depth of cut is below the critical value, that is to say, 54.63 nm and the removal of material is dominated by plastic flow.

IV. CONCLUSION

In this research, polishing tests of blanket silicon wafers with an ice polishing pad containing nano-sized Al_2O_3 slurry were carried out to investigate the polishing effect and mechanism. The following conclusions can be drawn:

(i) Nano-sized powders of Al_2O_3 were collocated into polishing slurry and then the polishing slurry froze to form an ice polishing pad. With the ice polishing pad, a super smooth surface with an average roughness of 0.367 nm is obtained within 1000 nm×1000 nm and there is a perfect silicon diamond structure without any microcracks in the subsurface.

(ii) Because the size of 60 nm CeO_2 is very small and there exists a soft corrosion layer and a stable thin liquid film between the silicon wafer and the ice pad during polishing, the cutting depth of the abrasive decreases. This proves the grain depth of the cut to be below the critical value, so the removal of material must be dominated by plastic flow

(iii) The IFA-PP has the ability of self-dressing. The chemical corrosion and mechanical removal act simultaneously during the ice polishing of silicon wafers.

V. ACKNOWLEDGMENTS

This work was supported by the Natural Science Foundation of Jiangsu Province in China (No.BK2005215), Graduate Innovation Foundation of Jiangsu Province (CX07B_066z), Foundation of the State Key Laboratory of Tribology of Tsinghua University and the National Natural Science Foundation of China (No.50675104). The authors gratefully thank Researcher M. R. Ji and J. X. Wu of University of Science and Technology of China and Prof. Y. G. Meng and Senior Engineer Y. Gao of Tshinghua University for their kind help in measurements.

[1] H. Fusstter, Mat. Res. Soc. Symp. Proc. **386**, 97 (1995).
[2] O. H. Peter, Microelectronic Engineering. **56**, 3 (2001).

DOI:10.1088/1674-0068/20/06/643-648

[3] H. K. Tönshoff, W. V. Schmiden, I. Inasaki, W. König, and G. Spur, Abrasive Machining of Silicon **39**, 621 (1990).
[4] E. Mendel, Solid State Tech. **10**, 27 (1967).
[5] Y. L. Liu, K. L. Zhang, F. Wang, and W. G. Di, Microelctronic Engineering **66**, 438 (2003).
[6] R. C. Liu, C. S. Pai, and E. Martinez, Solid-State Electronic **43**, 1003 (1999).
[7] T. Swetha, K. S. Arun, and K. Ashok, J. Electrochem. Soc. **151**, G205 (2004).
[8] I. Ali, Solid State Technol. **34**, 63 (1994).
[9] H. Lei, J. B. Luo, and J. J. Ma, Lubrication Engineering **4**, 74 (2002).
[10] Y. W. Zhao, L. Chang, and S. H. Kim, Wear **254**, 332 (2003).
[11] H. Lei and J. B. Luo, Wear. **257**, 461 (2004).
[12] X. A. Fu, C. A. Zorman, and M. Mehregany, J. Electrochem. Soc. **149**, 643 (2002).
[13] S. W. Park, C. B. Kim, and S. Y. Kim, Microelectronic Engineering **66**, 488 (2003).
[14] T. Hoshino, Y. Kurta, and Y. Terasaki, J. of Non-Crystalline Solids **283**, 129 (2001).
[15] E. K. Sanchez, S. Ha, and J. Grim, J. Electrochem. Soc. **149**, 131 (2002).
[16] T. W. Kim and Y. J. Cho, Tribology International. **39**, 1388 (2006).
[17] L. Chang, J. of Tribology **129**, 436 (2007).
[18] L. Cook, J. Non-Crystalline Solids **120**, 152 (1990).
[19] Z. Stavreva, D. Zeidler, M. Plotner, and K. Drescher, Appl. Surf. Sci. **108**, 39 (1997).
[20] S. Runnels, J. Electrochem. Soc. **141**, 1900 (1999).
[21] S. Paul, P. P. Bandyopadhyay, and A. B. Chattopadhyay, J. Mater. Proc. Technol. **37**, 791 (1993).
[22] J. Warnock, Electrochem. Soc. **138**, 2398 (1991).
[23] X. Y. Liu, L. J. Wang, C. F. Gao, X. S. Wu, and W.N. Liu, Chin. J. of Mechanical Engineering **38**, 47 (2002).
[24] R. J. Han, G. S. An, Y. W. Liu, S. Pei, R. Liang, Y. Zhang, J. S. Wu, and L. J. Wang, Aviation Precision Manufacturing Technology **35**, 1 (1999).
[25] R. J. Han, H. D. Sun, and D. Q. Xu, Optics and Precision Engineering **6**, 104 (1998).
[26] X. D. Li, B. Bhushan, and K. Takashima, Ultramicroscopy **97**, 481 (2003).
[27] B. Bhushan, *Handbook of Micro/Nanotribology*, Boca Raton: CRC Press, 136 (1999).
[28] B. Bhushan, *Modern Tribology Handbook*, Boca Raton: CRC Press, 826 (2001).
[29] X. Li and B. Bhushan, J. Mater. Res. **14**, 2328 (1999).
[30] S. H. Li, C. H Zhou, and R. J. Zhang, Tribology **22**, 74 (2002).
[31] Q. J. Xue and W. M. Liu, Pro. in Chem. **9**, 311 (1997).
[32] D. Graf, A. Schnegg, and R. Schmolke, Electrochem. Soc. Proc. **96**, 186 (2000).
[33] T. G. Bifnao, T. A. Bow, and R. O. Scattergood, J. Eng. Industry **113**, 184 (1991).

DOI:10.1088/1674-0068/20/06/643-648